Marginal Fermi Liquid Theory in the Hubbard Model

Y. Kakehashi* and P. Fulde

Max-Planck-Institut für Physik komplexer Systeme, Nöthnitzer Str. 38, D-01187 Dresden, Germany

(Received 8 December 2004; published 18 April 2005)

We find marginal-Fermi-liquid- (MFL) like behavior in the Hubbard model on a square lattice for a range of hole doping and on-site interaction parameter U. Thereby we use a self-consistent projection operator method. It enables us to compute the momentum and frequency dependence of the single-particle excitations with high resolution. The Fermi surface is found to be holelike in the underdoped regime and electronlike in the overdoped regime. Our calculations concern normal state properties of the system. When a comparison is possible, we find consistency with finite temperature quantum Monte Carlo results. We also find a discontinuous change with doping concentration from a MFL to a Fermi-liquid behavior resulting from a collapse of the lower Hubbard band. This renders Luttinger's theorem inapplicable in the underdoped regime.

DOI: 10.1103/PhysRevLett.94.156401 PACS numbers: 71.10.–w, 71.18.+y, 74.72.–h, 79.60.Bm

After the discovery of high-temperature superconductivity in layered Cu-based perovskites it was found that those materials exhibit quite unusual properties in the normal state. For example, in underdoped materials, i.e., for hole concentrations less than the one leading to the highest superconducting transition temperature, the temperature-dependent resistivity is found to be $\rho(T) \sim T$ in the normal state. Also, the nuclear relaxation rate, e.g., of $YBa_2Cu_3O_7$ has an unusual temperature independent contribution.

Aiming for an explanation of these strong deviations from a normal metal behavior, Varma *et al.* [1] developed the marginal-Fermi-liquid (MFL) theory. This theory assumes that the frequency ω and temperature T dependent self-energy $\Sigma(\omega, T)$ of the electrons behaves for $\omega > T$ like $\mathrm{Re}\,\Sigma(\omega, T) \sim \omega \ln|\omega|$ and $\mathrm{Im}\,\Sigma(\omega, T) \sim |\omega|$ in contrast to ordinary Fermi-liquid theory where $\mathrm{Re}\,\Sigma(\omega, T) \sim \omega$ and $\mathrm{Im}\,\Sigma(\omega, T) \sim \omega^2$ holds. Note that at zero temperature, the MFL form of the self-energy implies a diverging effective mass at the Fermi energy. With these assumptions most of the observed strong deviations from normal metal behavior could be explained surprisingly well. However, the microscopic origin of MFL behavior of the self-energy has remained an open problem.

There have been detailed studies of the two-dimensional (2D) Hubbard model as a simple model for the high-T_c cuprates [2] mainly by using advanced numerical techniques. We mention, in particular, the Lanczos method [2], the quantum Monte Carlo (QMC) [3–5] method, or calculations based on the dynamical cluster approximation (DCA) [6].

A perturbation analysis of the half-filled case at $T = 0$ has shown that in the weak Coulomb interaction limit, a MFL type of self-energy is obtained [7]. It is due to the van Hove singularities, which one is dealing with in this particular case. But we know that electron correlations are strong in the superconducting cuprates and that at $T = 0$ the system is an antiferromagnet [2,5,8]. It is also known that by hole doping the antiferromagnetic correlations are rapidly suppressed [2,5,6,9]. Nevertheless MFL behavior continues to exist in the underdoped regime and the question is whether or not it can be explained within the 2D Hubbard model with fairly strong interactions.

The aim of this Letter is to demonstrate that MFL behavior can indeed be derived from a doped 2D Hubbard model on a square lattice at $T = 0$ and large on-site interaction. This has become possible with the help of a recently developed self-consistent projection operator method (SCPM) [10]. It allows for high resolution calculations of the self-energy in regards to its momentum and energy and avoids certain problems previous numerical calculations have had to face. Our calculations deal with normal state properties, i.e., in case that the model yields a superconducting ground state they apply to temperatures larger than the transition temperature.

The SCPM is an extension to the nonlocal case of a projection operator coherent potential approximation (CPA) [11]. The latter was shown to be equivalent to the many-body CPA, the dynamical CPA, as well as the dynamical mean-field theory [12]. In the following, we outline briefly the main equations which are used before we present the numerical results demonstrating MFL behavior. More detailed derivations of the equations are found in the original literature [10–12].

The starting point is the retarded Green function

$$G_{\boldsymbol{k}}(z) = \frac{1}{z - \epsilon_{\boldsymbol{k}} - \Lambda_{\boldsymbol{k}}(z)}. \tag{1}$$

Here $z = \omega + i\delta$, where δ is a positive infinitesimal number, $\epsilon_{\boldsymbol{k}}$ is the Hartree-Fock one-electron dispersion measured from the Fermi energy, and $\Lambda_{\boldsymbol{k}}(z)$ is the self-energy calculated from the nonlocal memory matrix M_{ij} according to

$$\Lambda_{\boldsymbol{k}}(z) = U^2 \sum_j M_{j0}(z) \exp(i\boldsymbol{k} \cdot \boldsymbol{R}_j). \tag{2}$$

While U denotes the Hubbard on-site interaction, $\boldsymbol{R}_j$ is the

position vector of site j. We calculate $M_{ij}(z)$ by using an incremental cluster expansion up to two-sites contributions

$$M_{ii}(z) = M_{ii}^{(i)}(z) + \sum_{l\neq i}[M_{ii}^{(il)}(z) - M_{ii}^{(i)}(z)], \tag{3}$$

$$M_{i\neq j}(z) = M_{i\neq j}^{(ij)}(z), \tag{4}$$

where $M_{ii}^{(i)}(z)$ and $M_{i\neq j}^{(ij)}(z)$ are matrix elements of the cluster memory matrices $M_{lm}^{(c)}(z)$ $(c = i, ij)$. The latter can be expressed in terms of a "screened memory matrix" $\hat{\boldsymbol{M}}^{(c)}(z)$ and a matrix $\boldsymbol{L}^{(c)}(z)$ which describes on-site excitations. It is

$$M_{lm}^{(c)}(z) = [\hat{\boldsymbol{M}}^{(c)}(1 - \boldsymbol{L}^{(c)} \cdot \hat{\boldsymbol{M}}^{(c)})^{-1}]_{lm}. \tag{5}$$

The matrices have dimensions 1×1 when $c = i$ and 2×2 when $c = (ij)$. Specifically, $L^{(i)}(z) = U(1 - 2\langle n_{i-\sigma}\rangle)/[\langle n_{i-\sigma}\rangle(1 - \langle n_{i-\sigma}\rangle)]$ while $\boldsymbol{L}^{(ij)}(z)$ is a diagonal matrix with elements $L^{(i)}(z)$ and $L^{(j)}(z)$. As usual, $\langle n_{i\sigma}\rangle$ is the average electron number at site i with spin σ. The screened memory matrix is calculated from renormalized perturbation theory [13] as

$$\hat{M}_{ij}^{(c)}(z) = A_{ij} \times \int \frac{d\epsilon d\epsilon' d\epsilon'' \tilde{\rho}_{ij}^{(c)}(\epsilon)\tilde{\rho}_{ij}^{(c)}(\epsilon')\tilde{\rho}_{ji}^{(c)}(\epsilon'')\chi(\epsilon, \epsilon', \epsilon'')}{z - \epsilon - \epsilon' + \epsilon''}, \tag{6}$$

with $A_{ii} = [\langle n_{i-\sigma}\rangle(1 - \langle n_{i-\sigma}\rangle)]/[\langle n_{i-\sigma}\rangle_c(1 - \langle n_{i-\sigma}\rangle_c)]$ and $A_{i\neq j} = 1$. Here $\langle n_{i\sigma}\rangle_c = \int d\epsilon \tilde{\rho}_{ii}^{(c)}(\epsilon) f(\epsilon)$, with $f(\epsilon)$ denoting Fermi's distribution. The matrix $\tilde{\rho}_{ij}^{(c)}(\epsilon)$ describes the density of states of a system with an empty site i (or sites i and j) embedded in a medium with a coherent potential $\tilde{\Sigma}(z)$. This coherent potential is determined self-consistently from $\tilde{\Sigma}(z) = N^{-1}\sum_{\boldsymbol{k}}\Lambda_{\boldsymbol{k}}(z)$, where N is the number of sites. Moreover, $\chi(\epsilon, \epsilon', \epsilon'') = f(-\epsilon) \times f(-\epsilon')f(\epsilon'') + f(\epsilon)f(\epsilon')f(-\epsilon'')$. We want to emphasize that in Eqs. (2)–(4) all memory matrices with site i separated sufficiently far from site j are taken into account until convergency is obtained.

It follows from Eqs. (5) and (6) that the self-energy reduces in the limit of small U to second-order perturbation theory while in the limit of large U the exact result of the atomic limit is reproduced [10]. Although the above computational scheme looks at first sight somewhat difficult to handle, this is not really the case. In fact, it allows us to calculate the self-energy directly without having to do a numerical analytic continuation or an interpolation in $\boldsymbol{k}$ space. Therefore, we obtain for it a high resolution in energy and momentum. In the numerical calculations we have done, we assumed a paramagnetic ground state since the antiferromagnetism is suppressed away from half filling. Whenever possible, we have made comparisons with quantum QMC results and the agreement was always very satisfactory.

In Fig. 1 the momentum-dependent excitation spectrum is shown in the underdoped case for $U = 8$ (in units of the nearest-neighbor transfer integral) and $T = 0$. One notices an empty upper Hubbard band centered around the M point and a flat quasiparticle band crossing the Fermi energy ϵ_F. There is also incoherent spectral density near the Γ point resulting from the lower Hubbard band. Also shown are QMC results for finite temperatures [5]. Results for the Fermi surface are shown in Fig. 2. For $n = 0.95$ (underdoped case), a holelike Fermi surface is obtained. Because of a collapse of the lower Hubbard band the portion of the flat band around the X points sinks below the Fermi level. In the overdoped regime the Fermi surface is electronlike. It is seen that Luttinger's theorem [14] does not apply here. These results agree with the ones obtained from the DCA [6] and the QMC [5]. They are at variance with Ref. [15] where it is said that the shape of the Fermi surface is independent of U [15].

By taking numerical derivatives of $\Lambda_{\boldsymbol{k}}(z)$ we have determined the momentum-dependent effective mass $m_{\boldsymbol{k}} = 1 - \partial \mathrm{Re}\,\Lambda_{\boldsymbol{k}}(0^+)/\partial\omega$ in the underdoped regime (see Fig. 3). To our knowledge, this is something which could not be done before. For doping less than 2% $m_{\boldsymbol{k}}$ changes strongly between the minimum value at the M point and the maximum value at the X point, while for dopings larger than 2% the momentum dependence of $m_{\boldsymbol{k}}$ is weak with a maximum at Γ and not at X as in the underdoped regime. Most important is the strong dependence of $m_{\boldsymbol{k}}$ near the X point on the chosen step size $\delta\omega$ when the derivative is taken. This is a clear signature of MFL behavior. Because of the numerical derivative taken of $\mathrm{Re}\,\Lambda_{\boldsymbol{k}}$ at $\omega = 0$, we obtained a finite value of $m_{\boldsymbol{k}} \sim \ln\delta\omega$ instead of a divergency. In fact, in the limit of vanishing hole doping (half-

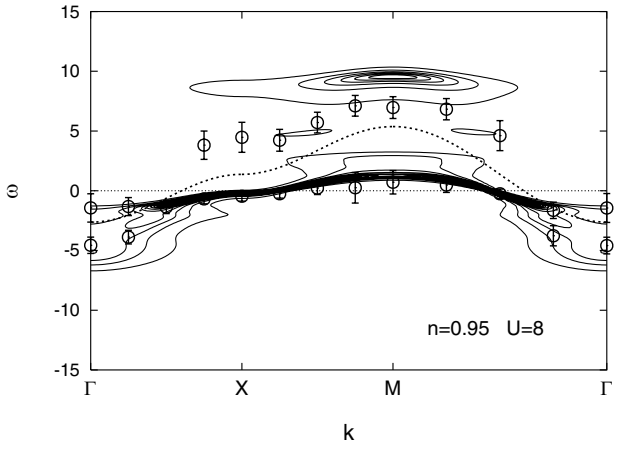

FIG. 1. Single-particle excitation spectra along high symmetry line for $U = 8$ and $T = 0$ in unit of the nearest-neighbor transfer integral: electron occupation number $n = 0.95$. Open circles with error bars are the QMC results [5] at $T = 0.33$. The dashed curves show the Hartree-Fock contribution ϵ_k.

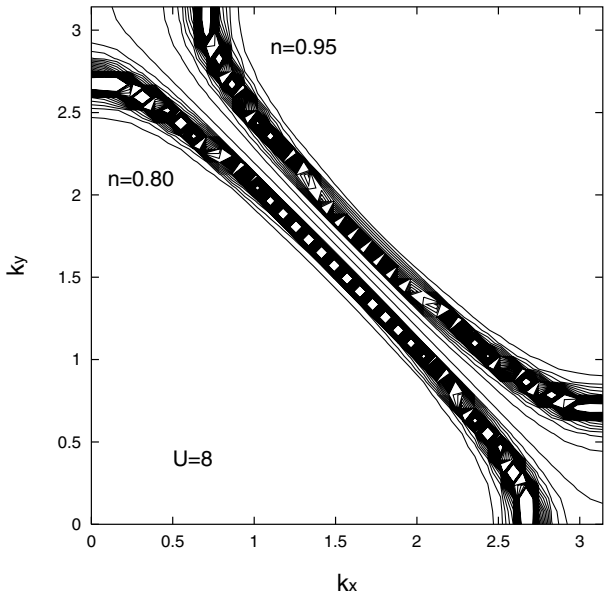

FIG. 2. Excitation spectra at the Fermi energy showing Fermi surfaces for $n = 0.95$ and 0.80. A 80×80 mesh was used for calculations in the Brillouin zone.

filled case) we find a typical MFL behavior of $\Lambda_{\boldsymbol{k}}(z)$ for $U = 8$ and $\boldsymbol{k} = (\pi/2, \pi/2)$ like in the weak interaction limit. This is shown in Fig. 4 where the two cases are compared. Because of these features we conclude that for $U = 8$ and doping less than 2%, MFL theory applies, while for doping concentrations of more than 2%, normal Fermi-liquid theory is valid.

The different nature of the states for doping concentrations $\delta_h < 0.02$ and $\delta_h > 0.02$ is clearly seen in the density

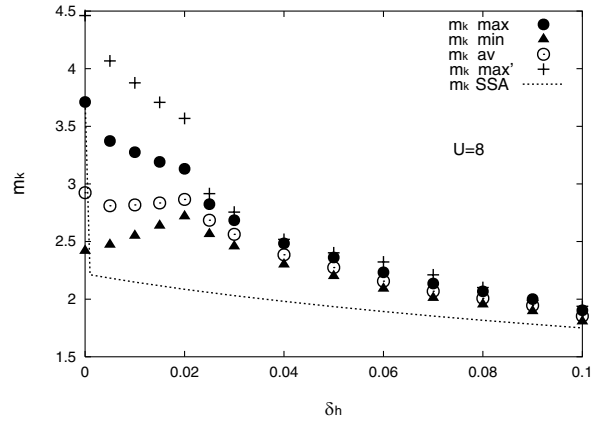

FIG. 3. Momentum-dependent effective mass $m_{\mathbf{k}}$ as a function of doping concentration. Closed circles: maximum value of $m_{\mathbf{k}}$ at $X(\pi, 0)$ for the hole concentration $\delta_h = 1 - n \leq 0.02$ and Γ $(0, 0)$ for $0.02 \leq \delta_h$; open circles: average $m_{\mathbf{k}}$; closed triangles: minimum value at $M(\pi, \pi)$. Numerical derivatives are taken with respect to energy fraction $\delta\omega = 0.05$. For the maximum $m_{\mathbf{k}}$, results for $\delta\omega = 0.005$ are also shown (+). The momentum-independent effective mass in the single-site approximation (SSA) is shown by the dashed curve.

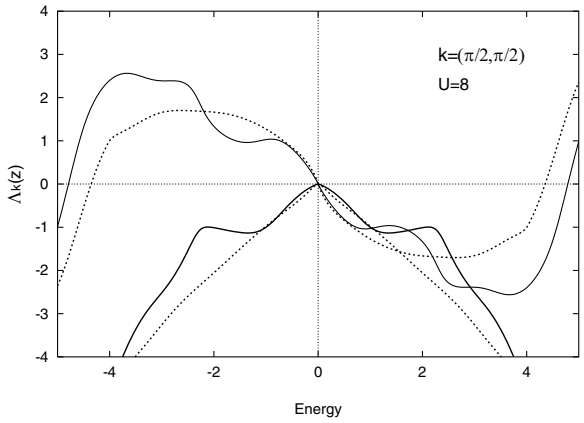

FIG. 4. Real part (thin solid line) and imaginary part (solid line) of the self-energy at the k point $(\pi/2, \pi/2)$ and half filling. Corresponding results of second-order perturbation theory are shown by dashed lines.

of states (DOS) presented in Fig. 5 for $U = 8$. Consider first the case $\delta_h < 0.02$. With increasing doping concentration, spectral density is shifted from the lower to the upper Hubbard band, or more generally to higher energies. As a consequence, the peak in the DOS remains at ϵ_F; i.e., it does not shift for small doping concentrations. Therefore, the self-energy has to good approximations the same frequency dependence as for half filling. This is the origin of MFL behavior. When $\delta_h > 0.02$ the lower Hubbard band has essentially collapsed and the peak in the DOS moves away from ϵ_F. In that case, conventional Fermi-liquid behavior sets in. This occurs in a rather discontinuous way. This is seen from the phase diagram shown in Fig. 6. The MFL regime with a still existing lower Hubbard band is separated by a region in which two self-consistent

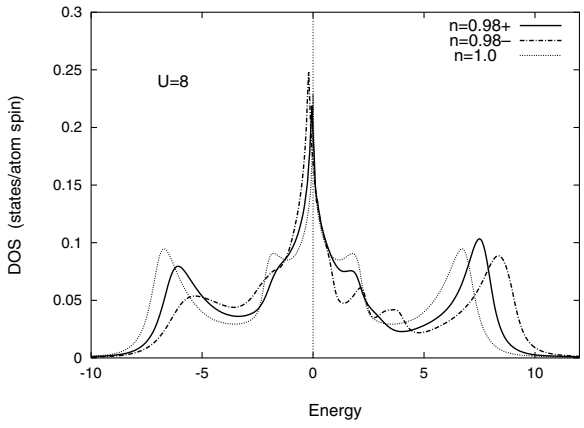

FIG. 5. Densities of states (DOS) for the two self-consistent solutions at $n = 0.98$. One $n = 0.98+$ (solid curve) is smoothly connected with the region $n \geq 0.98$, while the other $n = 0.98-$ (dot-dashed curve) with the region $n \leq 0.98$. The DOS for $n = 1$ is also shown (dotted line). Note that $\delta = 0.02$ (imaginary part of energy) was used in the numerical calculations so that the peak at $\omega = 0$ remains finite for $n = 1$.

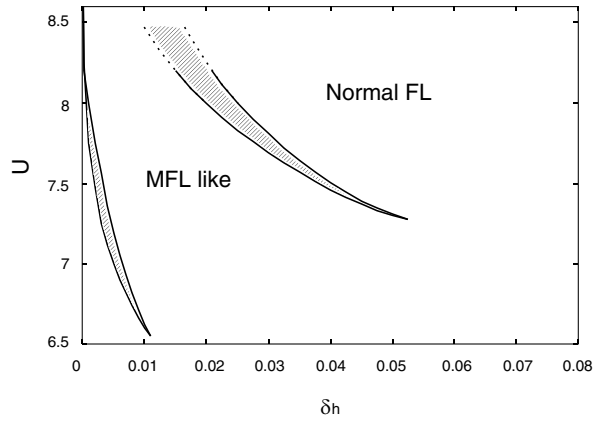

FIG. 6. Phase diagram showing discontinuity lines. The different transition lines are explained in the text. The regimes with two self-consistent solutions are shown by hatched areas. Dashed lines are extrapolations.

solutions are found from the one with a collapsed lower Hubbard band. One may consider that transition as one from quasilocalized electrons to fully itinerant ones. Note that when $\delta_h < 0.01$ the MFL regime is divided into two regimes. The two solutions found are only slightly different in the amount of the reduction of the lower Hubbard band. For fixed value of δ_h the discontinuous behavior of the self-energy as function of U implies that Luttinger's theorem [14] is not applicable. For $U < 6.5$ the MFL behavior at half filling changes smoothly to a Fermi-liquid state.

In summary, by using the SCPM we could calculate the zero-temperature self-energy $\Lambda_{\boldsymbol{k}}(z)$ for the 2D Hubbard model with high resolution with respect to ω and $\boldsymbol{k}$. We find a MFL-like behavior for quite a large range of hole doping concentration and $U(\gtrsim 7.3)$. We obtain there a strong momentum dependence of the effective mass. In cases where a comparison with finite temperature results [3–6] can be made, the agreement is good. When $U > 6.5$ a discontinuous change takes place with increasing hole concentration from more localized electrons in the lower Hubbard band to fully itinerant ones. In the latter case the lower Hubbard band is absent. It is precisely the transfer of spectral density from the lower Hubbard band to higher energies which results in MFL behavior at low hole concentrations. Above the upper discontinuity lines Luttinger's theorem is not applicable. Very close to half filling, long-ranged antiferromagnetic correlations are expected to modify the present results. Those correlations have been neglected here.

*Present address: Department of Physics and Earth Sciences, Faculty of Science, University of Ryukyus, 1 Senbaru, Nishihara, Okinawa, 903-0213 Japan.

[1] C. M. Varma, P. B. Littlewood, and S. Schmitt-Rink, E. Abrahams, and A. E. Ruckenstein, Phys. Rev. Lett. **63**, 1996 (1989).
[2] E. Dagotto, Rev. Mod. Phys. **66**, 763 (1994); M. Imada, A. Fujimori, and Y. Tokura, Rev. Mod. Phys. **70**, 1039 (1998).
[3] N. Bulut, D. J. Scalapino, and S. R. White, Phys. Rev. Lett. **73**, 748 (1994); **72**, 705 (1994); Phys. Rev. **50**, 7215 (1994).
[4] R. Preuss, W. Hanke, and W. von der Linden, Phys. Rev. Lett. **75**, 1344 (1995).
[5] C. Gröber, R. Eder, and W. Hanke, Phys. Rev. B **62**, 4336 (2000).
[6] Th. A. Maier, Th. Pruschke, and M. Jarrell, Phys. Rev. B **66**, 075102 (2002).
[7] A. Virosztek and J. Ruvalds, Phys. Rev. B **42**, 4064 (1990); H. Schweitzer and G. Czycholl, Z. Phys. B **83**, 93 (1991); G. Kastrinakis, Physica C (Amsterdam) **340**, 119 (2000).
[8] M. Jarrell, Th. Maier, C. Huscroft, and S. Moukouri, Phys. Rev. B **64**, 195130 (2001).
[9] S. Onoda and M. Imada, J. Phys. Soc. Jpn. **70**, 3398 (2001).
[10] Y. Kakehashi and P. Fulde, Phys. Rev. B**70**, 155112 (2004).
[11] Y. Kakehashi and P. Fulde, Phys. Rev. B **69**, 045101 (2004).
[12] Y. Kakehashi, Adv. Phys. **53**, 497 (2004).
[13] We adopted here the self-energy with parameters $(\lambda, \lambda') = (0, 1)$ in Eq. (53) of Ref. [10].
[14] J. M. Luttinger and J. C. Ward, Phys. Rev. **118**, 1417 (1960).
[15] B. Farid, Phil. Mag. **83**, 2829 (2003).